

1 **Modeling the growth and decline of pathogen effective**
2 **population size provides insight into epidemic**
3 **dynamics and drivers of antimicrobial resistance**

4 ERIK M. VOLZ¹ AND XAVIER DIDELOT¹

5 ¹*Department of Infectious Disease Epidemiology, Imperial College London,*
6 *Norfolk Place, W2 1PG, United Kingdom*

7 **Corresponding author:** Erik Volz, Department of Infectious Disease Epidemiology,
8 Imperial College London, Norfolk Place, W2 1PG, United Kingdom; E-mail:
9 e.volz@imperial.ac.uk

ABSTRACT

10

11 Non-parametric population genetic modeling provides a simple and flexible approach for
12 studying demographic history and epidemic dynamics using pathogen sequence data.
13 Existing Bayesian approaches are premised on stationary stochastic processes which may
14 provide an unrealistic prior for epidemic histories which feature extended period of
15 exponential growth or decline. We show that non-parametric models defined in terms of
16 the growth rate of the effective population size can provide a more realistic prior for
17 epidemic history. We propose a non-parametric autoregressive model on the growth rate as
18 a prior for effective population size, which corresponds to the dynamics expected under
19 many epidemic situations. We demonstrate the use of this model within a Bayesian
20 phylodynamic inference framework. Our method correctly reconstructs trends of epidemic
21 growth and decline from pathogen genealogies even when genealogical data is sparse and
22 conventional skyline estimators erroneously predict stable population size. We also propose
23 a regression approach for relating growth rates of pathogen effective population size and
24 time-varying variables that may impact the replicative fitness of a pathogen. The model is
25 applied to real data from rabies virus and *Staphylococcus aureus* epidemics. We find a close
26 correspondence between the estimated growth rates of a lineage of methicillin-resistant *S.*
27 *aureus* and population-level prescription rates of β -lactam antibiotics. The new models are
28 implemented in an open source R package called *skygrowth* which is available at
29 <https://mrc-ide.github.io/skygrowth/>.

30 (Keywords: phylodynamics, effective population size, growth rate, *skygrowth* ,
31 antimicrobial resistance, MRSA)

32 Non-parametric population genetic modeling has emerged as a simple, flexible,
33 popular and powerful tool for interrogating genetic sequence data to reveal demographic
34 history (Ho and Shapiro 2011). This approach has proved especially useful for analysis of
35 pathogen sequence data to reconstruct epidemic history and such models are increasingly
36 incorporated into surveillance systems for infectious diseases (Volz et al. 2013). The most
37 commonly used techniques are derivatives of the original *skyline* coalescent model, which
38 describes the evolution of effective population size as a piecewise constant function of time
39 (Pybus et al. 2000). The basic *skyline* model is prone to overfitting and estimating drastic
40 fluctuations in effective population size, so that numerous approaches were subsequently
41 developed for smoothing population size trajectories. Initial approaches to smoothing
42 *skyline* estimators were based on aggregating adjacent coalescent intervals within a
43 maximum likelihood framework (Strimmer and Pybus 2001). Subsequent development has
44 largely focused on Bayesian approaches where a more complex stochastic diffusion process
45 provides a prior for the evolution of a piecewise-constant function of effective population
46 size (Drummond et al. 2005). Non-parametric Bayesian approaches are now the most
47 popular approach for phylodynamic inference and such approaches have illuminated the
48 epidemic history of numerous pathogens in humans and animals (Ho and Shapiro 2011).

49 To date, all Bayesian non-parametric models have assumed that the effective
50 population size (or its logarithm) follows a stationary stochastic process such as a
51 Brownian motion (Minin et al. 2008; Palacios and Minin 2013). The choice of a stationary
52 process as prior can have large influence on size estimates especially when genealogical data
53 is sparse and uninformative. Genealogies often provide very little information about
54 effective population size near the present (or most recent sample), especially in
55 exponentially increasing populations (de Silva et al. 2012). In such cases, *skyline* estimators
56 with Brownian motion priors on the effective population size may produce estimates which
57 stabilize at a constant level even when the true size is increasing or decreasing

58 exponentially. We argue that in many situations, a more realistic prior can be defined in
59 terms of the growth rate of the effective population size. Below, we describe such a prior
60 based on a simple autoregressive stochastic process defined on the growth rate of effective
61 population size. We show how this prior can lead to substantially different estimates and
62 argue that these estimates are more accurate in many situations. When genealogical data is
63 sparse, our model will retain the growth rate learned from other parts of the genealogy and
64 will correctly capture trends of exponential growth or decline. Even though our approach is
65 non-parametric, we consider its relationship with parametric models of epidemic population
66 genetics to show that our estimates of growth rates of pathogen effective population size
67 are often likely to correspond to growth rates of an infectious disease epidemic.

68 Smoothing effective population size trajectories using a prior on growth rates also
69 has important advantages when incorporating non-genetic covariate data into
70 phylodynamic inference (Baele et al. 2016). Recent work has focused on refining effective
71 population size estimates using both the times of sequencing sampling (Karcher et al.
72 2016) or using environmental data which are expected to correlate with size estimates, such
73 as independent epidemic size estimates based on non-genetic data (Gill et al. 2016).
74 Existing statistical models have assumed that the effective population size has a linear or
75 log-linear relationship with temporal covariates. However in many cases, a more realistic
76 model would specify that the growth rate of effective population size is correlated with
77 covariates, as when for example an environmental variable impacts the replicative fitness of
78 a pathogen. We provide a similar extension of previous *skyride* models with covariate data
79 (Gill et al. 2016) to show how such data can be used to test hypotheses concerning their
80 effect and, when a significant effect exists, to refine estimates of both the growth rates and
81 the effective population sizes.

82 We illustrate the potential advantages of our growth rate model using a rabies virus
83 dataset that has been thoroughly studied using previous phylodynamic methods (Biek

84 et al. 2007; Gill et al. 2016). In particular, we show how our model correctly estimates a
85 recent decline in epidemic size whereas previous models mistakenly predict a stabilisation
86 of the epidemic prevalence. We also apply our methodology to a genomic dataset of
87 methicilin-resistant *Staphylococcus aureus* that had not formally been analysed using
88 phylodynamic methods (Uhlemann et al. 2014). We show how time series on prescription
89 rates of β -lactam antibiotics correlate strongly with growth and decline of the effective
90 population size, revealing the impact of antibiotic use on the emergence and spread of
91 resistant bacterial pathogens.

92 METHODS AND MATERIALS

93 We model effective population size through time as a first order autoregressive
94 stochastic process on the growth rate. This provides an intuitive link between the growth
95 rate of effective population size of pathogens and epidemic size as well as the reproduction
96 number of the epidemic. We further show how to incorporate time-varying environmental
97 covariates into phylodynamic inference.

98 *Previous Bayesian non-parametric phylodynamic models*

Several non-parametric phylodynamic models have been proposed based on Brownian motion (BM) processes and the Kingman coalescent genealogical model (Kingman 1982). In particular, the Bayesian non-parametric *skyride* model uses a BM prior to smooth trajectories of the logarithm of the effective population size (Minin et al. 2008). Let $\gamma(t) = \log(Ne(t))$ denote the logarithm of the effective population size as a function of time. The BM prior is defined as:

$$\gamma(t + dt) \sim \gamma(t) + \mathcal{N}(0, dt/\tau) \quad (1)$$

99 where τ is an estimated precision parameter, for which an uninformative Gamma prior is
100 typically used.

This BM prior has been adapted and applied in a variety of ways to enable statistical inference. In the *skygrid* model (Gill et al. 2012), time is discretized and γ is defined to be a piecewise constant function of time over a grid with time increments h , and the value γ_i is estimated for each interval i . Time intervals do not in general correspond to coalescent times in the genealogy. In this case, the BM prior is computed over increments of γ :

$$p(\gamma_{1:m}|\tau) \propto \prod_{i=1}^{m-1} p(\gamma_{i+1} - \gamma_i|\tau) \quad (2)$$

where

$$p(\gamma_{i+1} - \gamma_i|\tau) = \sqrt{\frac{\tau}{2\pi h}} e^{-\frac{\tau}{2h}(\gamma_{i+1} - \gamma_i)^2}$$

101 The genealogical data takes the form $\mathcal{G} = (c_{1:(n-1)}, s_{1:n})$ where c and s are
102 respectively ordered coalescent times (internal nodes of the genealogy) and sampling times
103 (terminal nodes of the genealogy). In the coalescent framework, the sampling times are
104 usually considered to be fixed, so that $p(s) = 1$ and $p(\mathcal{G}) = p(c|s)$. Alternatively, in some
105 variations of this model, a prior $p(s|Ne)$ is also provided for the sequence of sampling
106 times, making this approach similar to but more flexible than sampling-birth-death-models
107 (Karcher et al. 2016; Volz and Frost 2014).

Given a genealogy, the posterior distribution of the parameters τ and $\gamma_{1:m}$ is decomposed as:

$$p(\gamma_{1:m}, \tau|\mathcal{G}) \propto p(\mathcal{G}|\gamma_{1:m})p(\gamma_{1:m}|\tau)p(\tau) \quad (3)$$

108 The second term is given by Equation 2 and the last term by the prior on τ . To assist with

109 the definition of the first term, we first denote $A(t)$ to be the number of extant lineages at
110 time t :

$$A(t) = \sum_{i=1}^n I(s_i > t) - \sum_{i=1}^{n-1} I(c_i > t) \quad (4)$$

where $I(x)$ is an indicator function equal to one when x is true and equal to zero otherwise. The probability density of the genealogical data given the population size history $\gamma_{1:m}$ is then equal to (Griffiths and Tavaré 1994):

$$p(\mathcal{G}|\gamma_{1:m}) = \prod_{i=1}^{2n-2} \left(I(t_i \in c_i) \frac{\binom{A(t_i)}{2}}{\text{Ne}(t_{i+1})} e^{-\int_{t_i}^{t_{i+1}} -\left(\frac{A(t)}{2}\right) \frac{1}{\text{Ne}(t)} dt} \right. \\ \left. + (1 - I(t_i \in c_i)) e^{-\int_{t_i}^{t_{i+1}} -\left(\frac{A(t)}{2}\right) \frac{1}{\text{Ne}(t)} dt} \right) \quad (5)$$

111 where $t_{1:(2n-1)} = c_{1:(n-1)} \cup s_{1:n}$ is the set union of sample and coalescent times in descending
112 order.

113 *Relationship between the growth rate of effective population size and* 114 *epidemic properties*

115 Several recent studies have investigated the relationship between the effective population
116 size of a pathogen and the number of infected hosts (Koelle et al. 2011; Dearlove and
117 Wilson 2013; Rosenberg and Nordborg 2002). A simple link between these quantities does
118 not exist, since the relationship depends on how incidence and epidemic size change
119 through time (Volz et al. 2009), population structure (Volz 2012), and complex evolution of
120 the pathogen within hosts (Didelot et al. 2016; Volz et al. 2017). Under idealized
121 situations, there is however a simple relationship between the growth rate of effective
122 population size and the growth rate of an epidemic (Frost and Volz 2010; Volz et al. 2013).

123 Let $Y(t)$ and $\beta(t)$ denote the number of infected hosts and per-capita transmission
124 rate, respectively, as functions of time. Note that $\beta(t)$ may depend on the density of
125 susceptible individuals in the population, as in the common susceptible-infected-removed
126 (SIR) model, in which case $\beta(t) \propto S(t)/N$ (Allen 2008). The coalescent rate for an
127 infectious disease epidemic was previously derived under the assumption that within-host
128 effective population size is negligible and that super-infection does not occur (Volz et al.
129 2009; Frost and Volz 2010):

$$\lambda(t) = \binom{A(t)}{2} \frac{2\beta(t)}{Y(t)} \quad (6)$$

130 Equating this rate with the coalescent rate under the coalescent model $\lambda(t) = \binom{A(t)}{2} / \text{Ne}(t)$
131 (Kingman 1982) yields the following formula for the effective population size:

$$\text{Ne}(t) = \frac{Y(t)}{2\beta(t)} \quad (7)$$

132 Differentiating with respect to time (denoting with a dot superscript) yields:

$$\dot{\text{Ne}}(t) = \frac{\dot{Y}(t)}{2\beta(t)} - \frac{\dot{\beta}(t)Y(t)}{2(\beta(t))^2} \quad (8)$$

133 Note that in general the growth rate of the effective population size does not correspond to
134 the growth rate of Y , however if the per-capita transmission rate is constant ($\dot{\beta} = 0$), we
135 have $\dot{\text{Ne}} = \dot{Y}/(2\beta) \propto \dot{Y}$. Thus, we expect that over phases of the epidemic where
136 per-capita transmission rates are nearly constant there will be close correspondence
137 between the growth or decline of the effective population size and the growth or decline of
138 the unobserved number of infected hosts. This condition is often satisfied near the
139 beginning of an outbreak which has an exponential phase. It is also often satisfied towards
140 the end of epidemics when the epidemic size is decreasing at a constant exponential rate.

141 The basic reproduction number R_0 describes the expected number of transmission

142 events caused by a single infected individual in an otherwise susceptible population. By
143 extension, we can define $R(t)$ as the expected number of transmissions by an infected host
144 infected at time t (Fraser 2007). Assuming that all infected individuals are equally
145 infectious (as is the case for example in the SIR model), we have that during periods when
146 the epidemic growth rate is constant, each infected individual transmits at rate
147 $\beta(t) = R(t)/\psi$ where ψ is the mean duration of infections. With these definitions, the
148 number of infections $Y(t)$ varies according to the following differential equation:

$$\dot{Y}(t) = Y(t) \frac{R(t) - 1}{\psi} \quad (9)$$

149 Combining Equations 7, 8 and 9 leads to the following approximate estimator for
150 the reproduction number through time:

$$\hat{R}(t) = 1 + \psi \frac{\dot{N}e(t)}{N_e(t)} \quad (10)$$

151 This estimator makes use of the quantity $\dot{N}e(t)/N_e(t)$ which will be estimated in our model
152 below. Equation 10 is likely to be a good estimator over periods of the epidemic where
153 per-capita transmission rates are invariant. A special case of this occurs at the start of an
154 epidemic, in which case Equation 10 can be used to estimate the basic reproduction
155 number R_0 , as previously noted (Pybus 2001).

156 *A growth rate prior for effective population size*

157 We propose a model in which the growth rate of the effective population size is an
158 autoregressive process with stationary increments. This growth rate is defined as:

$$\rho(t) = \frac{\dot{N}e(t)}{N_e(t)} \quad (11)$$

159 Note that $\rho(t)$ is a real-valued quantity, with negative and positive values respectively
160 indicating an increase and decrease in the effective population size. In particular, if the
161 population is exponentially growing or declining from $t = 0$ then we have
162 $Ne(t) = Ne(0)\exp(\rho t)$ so that $\rho(t) = \rho$ at every time $t \geq 0$. More generally, we model $\rho(t)$
163 using a BM process: $\rho(t) \sim \text{BM}(\tau)$ (cf Equation 1). To facilitate statistical inference, we
164 work with a discretized time axis with m intervals of length h as in the *skygrid* model (Gill
165 et al. 2013). We define the growth rate in time interval i as:

$$\rho_i = \frac{Ne_{i+1} - Ne_i}{hNe_i} \quad (12)$$

166 We use the following approximate model for $p(\rho_{i+1}|\rho_i)$:

$$\rho_{i+1} \sim \rho_i + \mathcal{N}(0, h/\tau) \quad (13)$$

167 Note that Equation 12 implies $\rho_i \in (-1/h, \infty)$ since Ne cannot decline below zero, whereas
168 the approximate model in Equation 13 assumes support on the entire real line. We have
169 found performance with this approximate model to be superior to exact models on the log
170 transformation of Ne provided that h is small.

With the above definitions, the prior density of a sequence $\rho_{1:m}$ is defined in terms of the increments:

$$p(\rho_{1:m}|\tau) \propto \prod_{i=1}^{m-2} p(\rho_{i+1} - \rho_i|\tau) \quad (14)$$

where

$$p(\rho_{i+1} - \rho_i|\tau) = \sqrt{\frac{\tau}{2\pi h}} e^{-\frac{\tau}{2h}(\rho_{i+1}-\rho_i)^2}$$

171 This equation can be compared with the *skygrid* density, Equation 2.

172

Incorporating covariates into phylodynamic inference

A simple model was recently proposed for incorporating time-varying covariates into phylodynamic inference with *skygrid* models (Gill et al. 2016). Suppose we observe q covariates at m time points denoted $X = (X_{1:m,1:q})$, and such that observation times correspond to the grid used in the phylodynamic model. The following linear model for the marginal distribution of γ with covariate vector $\alpha_{1:q}$ was proposed:

$$p(\gamma_i|X, \alpha_{1:q}, \epsilon) \sim \mathcal{N}(\alpha_0 + X_{i,1:q}\alpha_{1:q}, \epsilon) \quad (15)$$

173 where α_0 is the expected mean of γ without covariate effects.

This implies, along with the BM model, the following marginal distribution of the increments:

$$p(\gamma_{i+1} - \gamma_i|X, \alpha_{1:q}, \tau, \epsilon) \sim \mathcal{N}(X_{i+1,1:q}\alpha_{1:q} - X_{i,1:q}\alpha_{1:q}, h/\tau + 2\epsilon) \quad (16)$$

When covariates are likely to be associated with growth rates of the effective population size instead of the logarithm of the effective population size, we can analogously define the density of increments of ρ :

$$p(\rho_{i+1} - \rho_i|X, \alpha_{1:q}, \tau, \epsilon) \sim \mathcal{N}(X_{i+1,1:q}\alpha_{1:q} - X_{i,1:q}\alpha_{1:q}, h/\tau + 2\epsilon) \quad (17)$$

174 When fitting this model, we drop ϵ for simplicity (as in Gill et al. 2016), and estimate a
175 single variance parameter τ .

176

Inference and software implementation

177 Our growth rate model is implemented in an open-source R package called *skygrowth*,
178 available from <https://mrc-ide.github.io/skygrowth/>, and which includes both

179 maximum a posteriori (MAP) and Bayesian Markov Chain Monte Carlo (MCMC) methods
180 for model fitting.

181 The MCMC procedure uses a Gibbs-within-Metropolis algorithm that alternates
182 between sampling the growth rate vector $\rho_{1:m}$ and sampling of the precision parameter τ .
183 Metropolis-Hastings sampling is also performed for regression coefficients $\alpha_{1:q}$ if covariate
184 data is provided with univariate normal proposals. The elements of $\rho_{1:m}$ are sampled in
185 sequence (from past to present), and multiple Gibbs iterations (by default one hundred)
186 are performed before updating other parameters using Metropolis-Hastings steps.

187 Maximum a posteriori (MAP) is used as a starting point for the MCMC. The MAP
188 estimator alternates between optimisation of $\gamma_{1:m}$ using gradient descent (*BFGS* in R,
189 Goldfarb 1970) and univariate optimisation of τ until convergence in the posterior is
190 observed. Approximate credible intervals are provided for the MAP estimator based on
191 curvature of the posterior around the optimum.

192 RESULTS

193 *Simulations*

194 We evaluated the ability of the *skygrowth* model to infer epidemic trends by simulating
195 partially-sampled genealogies from a stochastic individual-based
196 susceptible-infected-recovered (SIR) model. Simulated data were generated using the
197 BEAST2 package MASTER (Vaughan and Drummond 2013), and code to reproduce
198 simulated results is available at <https://github.com/emvolz/skygrowth-experiments>.
199 The *skygrowth* model was also compared to *skygrid* model as implemented in the *phylodyn*
200 R package (Karcher et al. 2016, 2017) which estimates effective population size using a fast
201 approximate Bayesian non-parametric reconstruction (BNPR). The SIR model was density

202 dependent with a reaction rate $\beta S(t)I(t)$ of generating new infections. Figure 1 shows
203 results of a single simulation with $R_0 = 1.3$ and 10,000 initial susceptible individuals.
204 Additional simulations are shown in supporting Figure S1. Estimates with *skygrowth* were
205 obtained using the MCMC algorithm and an Exponential(0.1) prior on the precision
206 parameter. We report the posterior means from both *skygrowth* and *skygrid* BNPR.
207 Genealogies were reconstructed by sampling 200 or 1000 infected individuals at random
208 from the entire history of the epidemic. In this scenario, both the *skygrowth* and
209 *skygrid* models reproduce the true epidemic trend, capturing both the rate of initial
210 exponential increase, the time of peak prevalence, and the rate of epidemic decline.
211 However, when sampling only 200 lineages (Figure 1A), the genealogy contains relatively
212 little information about later epidemic dynamics, and the *skygrid* estimates revert to a
213 stationary prior producing an unrealistic levelling-off of N_e . Estimates using the
214 *skygrid* BNPR model were highly similar to results using an exact MCMC algorithm for
215 sampling the posterior also included in the *phylodyn* package.

216 While the results in Figure 1A and B suggest that $N_e(t)$ can serve as a very effective
217 proxy for epidemic size, the degree of correspondence will depend on details of the epidemic
218 model as discussed in the Methods section. Figure 1C and supporting Figure S2 shows a
219 scenario where estimates of $N_e(t)$ capture the initial rate of exponential growth but fail to
220 estimate the time of peak epidemic prevalence, and the *skygrid* model also fails to detect
221 that the epidemic ever decreases. This scenario was based on a higher $R_0 = 5$ and only
222 2,000 initially susceptible individuals, such that almost all hosts are eventually infected and
223 the rate of epidemic decline predominantly reflects the host recovery rate. This is easily
224 understood using the formula $N_e(t) \propto I(t)/S(t)$ (cf. Equation 7). When R_0 is large, $S(t)$
225 will change drastically over the course of the epidemic. In the later stages, almost all hosts
226 have been infected so that $1/S(t)$ is large, producing correspondingly large effective
227 population sizes.

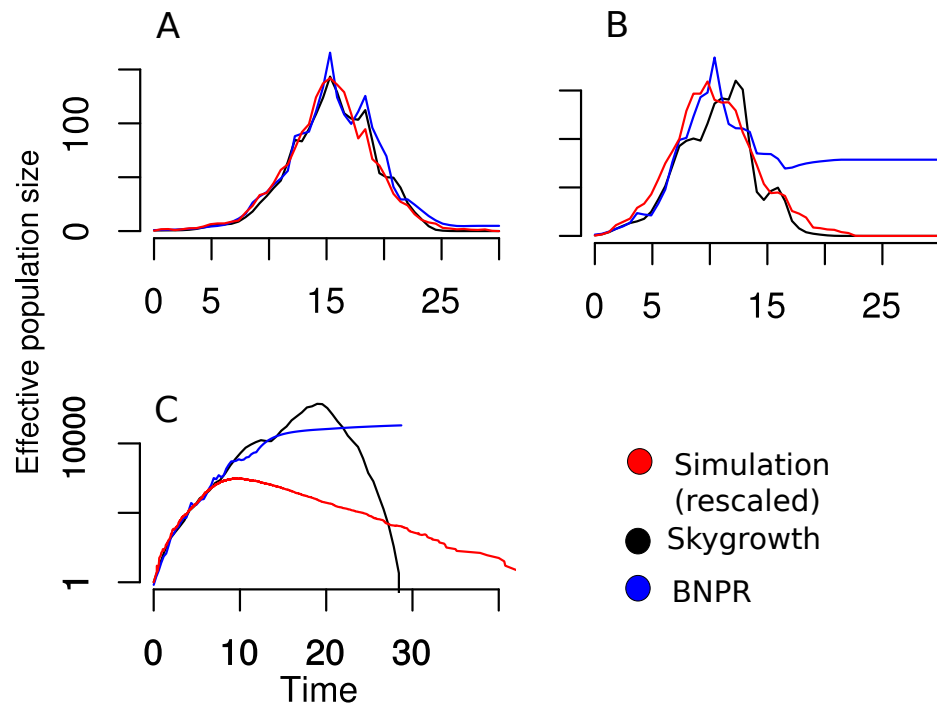


Figure 1: Comparison of effective population size estimates using the *skygrowth* and *skygrid* models applied to data from a susceptible-infected-recovered simulated epidemic. Effective population size estimates are also compared to the number of infected hosts through time under a linear rescaling (red). A. Estimates using a SIR model and simulated genealogy with 1000 sampled lineages and $R_0 = 1.3$. B. Estimates using a SIR model and simulated genealogy with 200 sampled lineages and $R_0 = 1.3$. C. Estimates using a SIR model and simulated genealogy with 200 sampled lineages and $R_0 = 5$.

228

Rabies virus

229 An epidemic of rabies broke out in the late 1970s in the North American raccoon
230 population, following the emergence of a host-adapted variant of the virus called RRV. By
231 the end of the 1990s, this outbreak had spread to a vast geographical area including all
232 Northeast and mid-Atlantic US states (Childs et al. 2000). A sample of 47 RRV isolates
233 has been sequenced in a previous study (Biek et al. 2007), and BEAST (Drummond et al.
234 2012) was used to reconstruct a dated phylogenetic tree. A standard *skyline* analysis
235 (Drummond et al. 2005) was performed, which visually suggested a correlation between the
236 inferred effective population size (N_e) and the monthly area newly affected by RRV
237 (hereafter denoted V), but without attempting to quantify the strength or significance of
238 this association.

239 This data was recently reanalysed using the *skygrid* model with covariates (Gill
240 et al. 2016). No significant association was found between N_e and V , but the authors noted
241 that since V is the newly affected area, V would be expected to be associated with a
242 change in N_e rather than N_e itself. Since the *skyride* method is focused on N_e , like all
243 previous phylodynamic methods, the authors considered the cumulative distribution of V
244 and showed that this is slightly associated with N_e (with a 95% credible interval of
245 [0.18-2.86] on the covariate effect size, Gill et al. 2016). However, this approach is not fully
246 satisfactory. In particular, since V is always positive, the cumulative distribution of V is
247 always increasing, whereas N_e is in principle equally likely to increase or decrease over
248 time. Furthermore both V and its cumulative distribution were considered on a logarithm
249 scale, so that the latter flattens over time by definition.

250 A more natural solution is to keep the covariate V untransformed, and investigate
251 its association with the growth rate $\rho(t)$ rather than $N_e(t)$ as implemented in our
252 methodology (Figure 2). For this analysis we used exactly the same dated phylogeny as
253 previously published (Biek et al. 2007) (reproduced in Supporting Figure S3). When the

254 covariate was not used (red results in Figure 2), the growth rate was inferred to be positive
255 but declining progressively to zero from 1973 to \sim 1983, then stable around zero up to
256 \sim 1990, followed by a period of positive growth until \sim 2000, after which the growth rate
257 decreased below zero. This implies that the effective population size increased from 1973 to
258 \sim 1983, then was stable until \sim 1990, increased to a peak in \sim 1997 and afterwards
259 decreased. Two waves of spread have therefore been inferred as in previous analyses (Biek
260 et al. 2007; Gill et al. 2016), with the first one starting in the 1970s and ending in \sim 1983
261 and the second one lasting from \sim 1990 to \sim 1997.

262 Unfortunately the covariate data V starts in September 1978 and therefore does not
263 cover the first wave. However, the covariate data shows that the epidemic was spreading
264 very quickly between 1992 and 1997, much faster than before or after these dates, and this
265 timing corresponds fairly precisely to the second wave of spread. When the covariate data
266 was integrated into phylodynamic inference, the covariate effect size was found to be
267 statistically significant but only slightly so, with a large 95% credible interval for the
268 covariate effect size of [0.03-4.61] and posterior mean of 1.09. The reconstructed growth
269 rate and effective population size when using the covariate data (blue results in Figure 2)
270 were compatible with results without covariate data. Using additional informative data
271 tightens the credible interval as would be expected, except in the second wave during which
272 the covariate data suggests higher values for both the growth rate and effective population
273 size. The mean posterior growth rate reached a value of about 2.5 per year in the 1990s
274 (Figure 2) and the average generation time of raccoon rabies has previously been estimated
275 to be around 2 months (Biek et al. 2007). We can use Equation 10 to infer a reproduction
276 number of $R = 1.4$, slightly higher than a previous estimate around $R = 1.1$ based on the
277 same data (Biek et al. 2007).

278 One of the main novel findings of our analysis is that we found a significant decline
279 of the effective population size of raccoon rabies post-2000, whereas previous phylodynamic

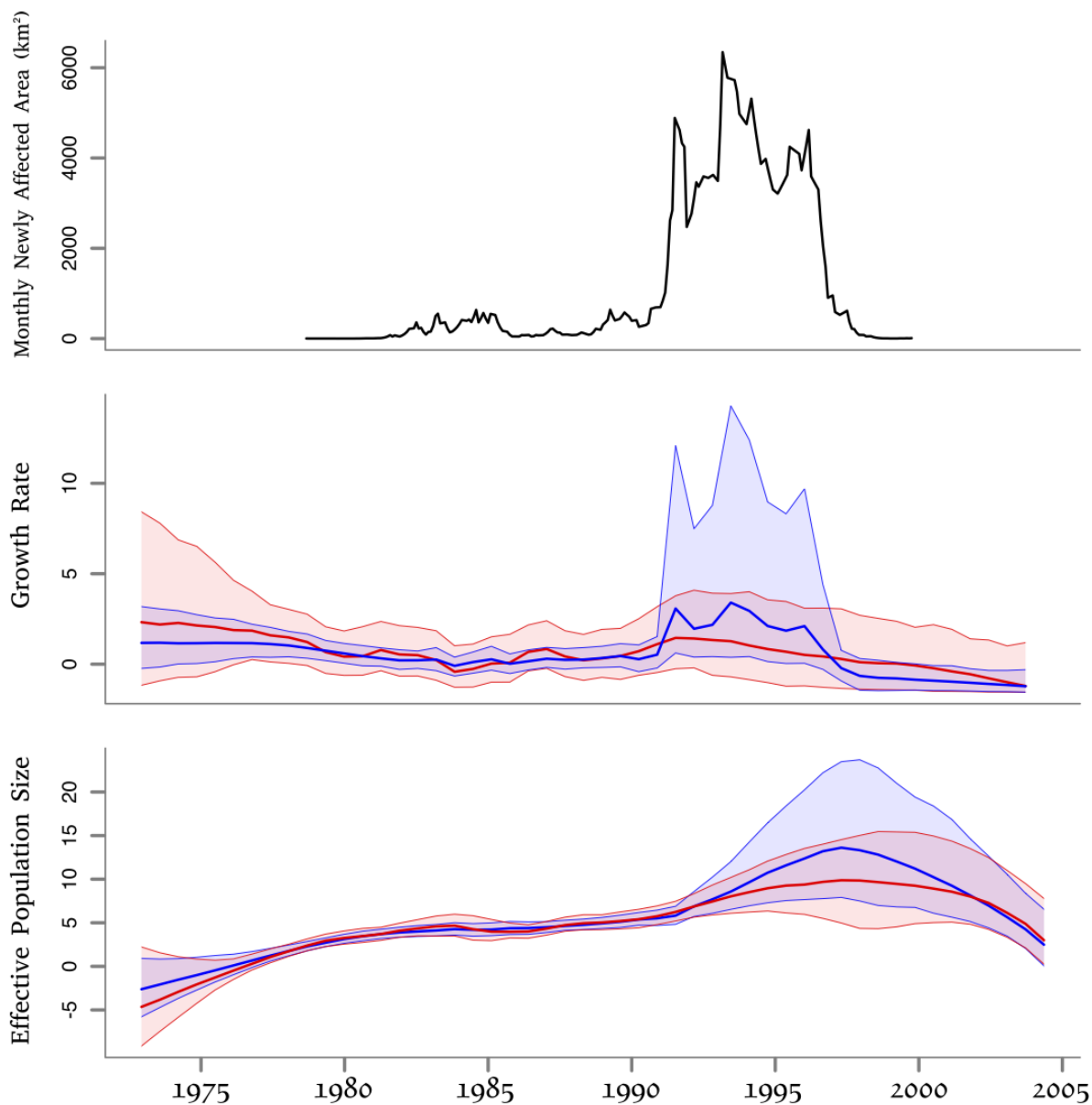


Figure 2: Results on the rabies application. Top: covariate data, representing the area in km² newly affected by rabies recorded monthly between September 1978 and October 1999. Middle: growth rate estimates. Bottom: log effective population size estimates. The middle and bottom plots show results without (red) and with (blue) the use of the covariate data, and with a solid line indicating posterior means and shaded areas indicating the 95% credible regions.

280 studies based on the same data found this to be constant (Biek et al. 2007; Gill et al.
281 2016). Previous methods consider a Brownian motion on the logarithm of N_e , which results
282 in a strong prior that N_e is constant in recent time. By contrast, our model results in the
283 growth rate being a-priori constant, so that the clear decline in growth rate started in the
284 mid-1990s is likely to have continued to the point that the growth rate became negative
285 and N_e declined. Our result is in good agreement with CDC surveillance that shows a clear
286 decline in rabid raccoons after the peak in the mid-1990s (Monroe et al. 2016).

287 *Staphylococcus aureus* USA300

288 *Staphylococcus aureus* is a bacterium that causes infections ranging from mild skin
289 infections to life-threatening septicaemia. In the 1980s and 1990s, several variants of *S.*
290 *aureus* have emerged that are resistant to methicilin and other β -lactam antibiotics, and
291 collectively called methicilin-resistant *S. aureus* (MRSA) (Chambers and Deleo 2009).
292 MRSA are well known as a leading cause of hospital infections worldwide, but the MRSA
293 variant called USA300 differs from most others by causing infections mostly in
294 communities rather than hospitals. USA300 was first reported in 2000, and has since
295 spread throughout the USA and internationally (Tenover and Goering 2009). A recent
296 study sequenced the genomes from 387 isolates of USA300 sampled from New York
297 between 2009 and 2011, and reconstructed phylogeographic spread that frequently involved
298 transmission within households (Uhlemann et al. 2014).

299 The USA300 phylogenetic tree (Uhlemann et al. 2014) was dated using a previously
300 described method (Didelot et al. 2012) and a clock rate of ~ 3 substitutions per year for
301 USA300 (Uhlemann et al. 2014; Alam et al. 2015). We analysed the resulting dated
302 phylogeny (Supporting Figure S4) using our phylodynamic methodology (Figure 3). We
303 initially performed this analysis without the use of any covariate data (red results in Figure
304 3) and found that the growth rate had been around zero up until 1985, after which it

305 steadily increased until \sim 1995, and subsequently decreased almost linearly, becoming
306 negative in \sim 2002 and continuing to decrease afterwards. The effective population size was
307 accordingly found to have been very small until the mid-1990s, to have peaked in \sim 2002
308 and to have declined since. These results are in very good agreement with a phylodynamic
309 analysis of USA300 performed using a traditional *skyline* plot on a different genomic
310 dataset (Glaser et al. 2016) as well as USA300 incidence trends (Planet 2017). However,
311 the causes for the recent decline in USA300 are still unclear (Planet 2017). Declines in
312 other MRSA lineages were recently described (Ledda et al. 2017) and have been attributed
313 to improved hospital infection control measures, but this does not apply to the
314 community-associated USA300 lineage.

315 We hypothesized that the dynamics of USA300 may be driven by the consumption
316 of β -lactams in the USA, and we therefore gathered data on this from three different
317 sources covering respectively the periods between 1980 and 1992 (McCaig and Hughes
318 1995), between 1992 and 2000 (McCaig et al. 2003) and between 2000 and 2012 (CDDEP
319 2017). There was an overlap of one year between the first and second, and between the
320 second and third of these sources, which was used to scale data for consistency between the
321 three sources. Specifically, values from the second source were scaled so that the 2000 value
322 is equal to the one in the third source, and values from the first source were then scaled so
323 that the 1992 value is equal to the one in the second source. The rescaled data is therefore
324 measured as in the third source, namely in standard units of β -lactams (ie narrow-spectrum
325 and broad spectrum penicilins plus cephalosporins) consumed per 1000 population in the
326 USA (CDDEP 2017). This data show that the consumption of β -lactams almost doubled
327 between 1980 and 1991, and subsequently decreased to reach around 2010 levels comparable
328 to the early 1980s (Figure 3). These trends on β -lactams consumption therefore appear to
329 be very similar to the ones observed for the USA300 growth rate without the use of
330 covariates (red results in Figure 3). To confirm this observation, we repeated our

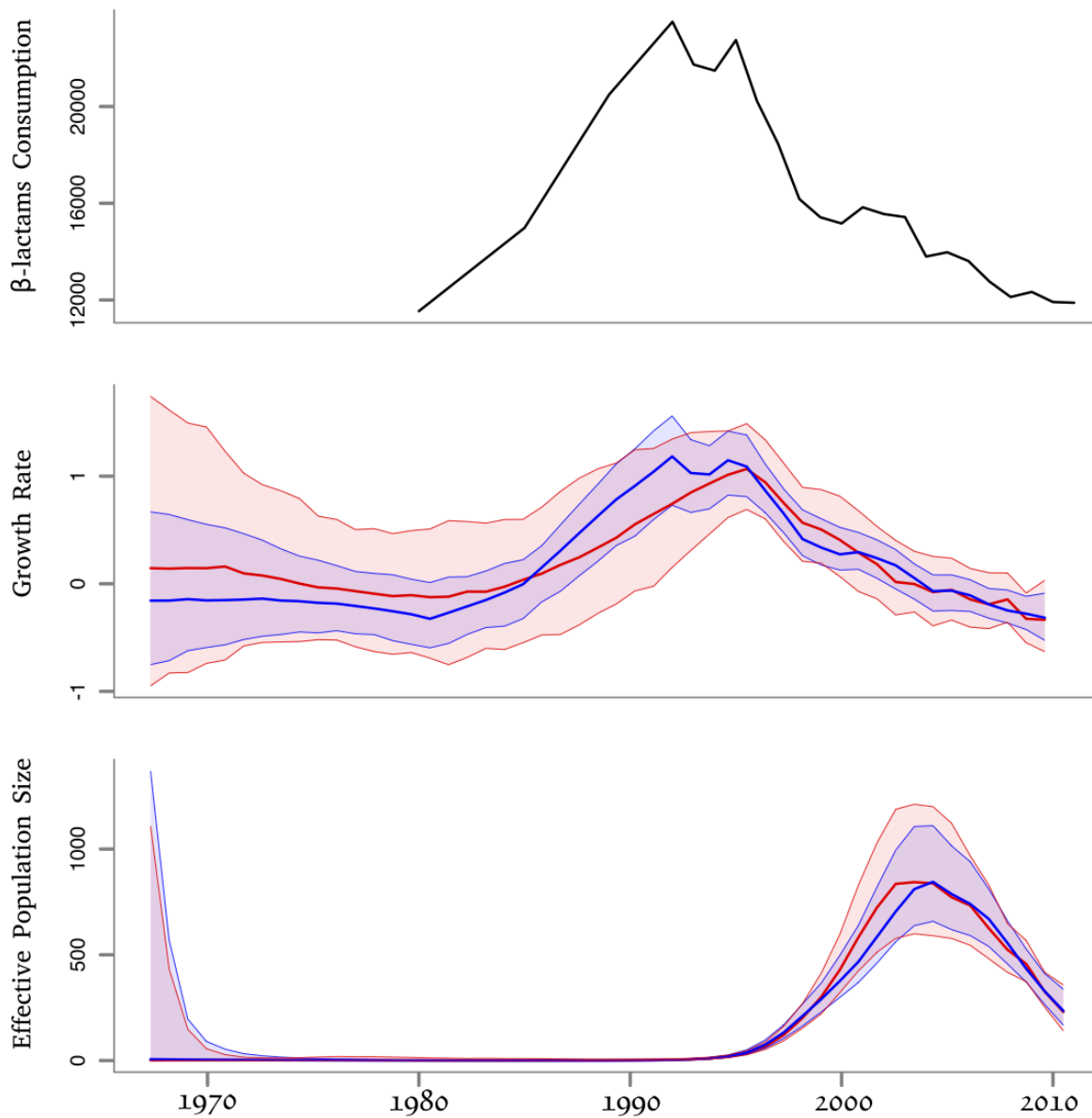


Figure 3: Results on the USA300 application. Top: covariate data, representing the consumption of β -lactams between 1980 to 2012 in the USA, measured in standard units per 1000 population. Middle: growth rate estimates. Bottom: log effective population size estimates. The middle and bottom plots show results without (red) and with (blue) the use of the covariate data, and with a solid line indicating posterior means and shaded areas indicating the 95% credible regions.

331 phylodynamic analysis with integration of the β -lactam use as a covariate (blue results in
332 Figure 3). We found that the covariate was significantly associated with growth rate, with
333 a mean posterior effect of 0.48 and 95% credible interval [0.18-0.71]. The growth rate
334 dynamics inferred when using covariate data was almost identical to those inferred without
335 the use of covariate data, except for a clear reduction of the width of the intervals which
336 reflects the gain in information when combining two independent types of data.

337 Our analysis therefore suggests that the rise in β -lactams consumption in the 1980s
338 was responsible for the emergence of the highly successful USA300 lineage. From the
339 mid-1990s, the use of β -lactams has declined, both due to an overall reduction in antibiotic
340 use and a diversification of the type of antibiotics prescribed (McCaig et al. 2003; CDDEP
341 2017), and the growth rate of USA300 has consequently decreased. Importantly, the
342 consumption of antibiotics is expected to be associated with the growth rates of resistant
343 bacterial pathogens, rather than with their effective population sizes, which here is not at
344 all correlated with the covariate (Figure 3). Amongst pairs of individuals thought to have
345 infected one another within households, the distribution of genomic distance had a mean of
346 4 substitutions (Uhlemann et al. 2014), and this represents on average twice the number of
347 substitutions occurring during an infection when accounting for within-host diversity
348 (Didelot et al. 2012, 2014, 2016). Given that the molecular clock rate of USA300 is
349 approximately 3 substitutions per year (Uhlemann et al. 2014; Alam et al. 2015), the
350 average duration of infections in this outbreak is around eight months. In the first half of
351 the 1990s, the growth rate peaked around 1 per year (Figure 3) and using Equation 10 we
352 estimate that the reproduction number was around $R = 1.6$, which is in good agreement
353 with the recent estimate $R = 1.5$ for MRSA in the US population (Hogea et al. 2014). The
354 fact that this estimate is only modestly above the minimum threshold of $R = 1$ required for
355 outbreaks to take place could help explain why the USA300 is declining, even though
356 β -lactams are still widely used. The consumption level may have lowered below the

357 threshold caused by the fitness cost of resistance, as previously discussed for other resistant
358 bacteria (Whittles et al. 2017; Dingle et al. 2017).

359 DISCUSSION

360 Many environmental covariates, particularly those with a mechanistic influence on
361 replicative fitness of pathogens, are closely related to the growth rate of epidemic size but
362 not necessarily related to absolute epidemic size. We have found that these relationships
363 can be inferred from random samples of pathogen genetic sequences by relating
364 environmental covariates to the growth rate of the effective population size. This enables
365 the estimation of the fitness effect of environmental covariates as well as the prediction of
366 future epidemic dynamics should conditions change. We have found a clear and highly
367 significant relationship between the growth and decline of community-associated MRSA
368 USA300 and the population-level prescription rates of β -lactam antibiotics (Figure 3). This
369 relationship is not apparent when comparing antibiotic usage directly with the effective
370 population size of MRSA USA300. Our methodology focused on growth rate is therefore
371 well suited to investigate the drivers of antibiotic resistance, compared to previous
372 phylodynamic methods focused on the effective population size.

373 The *skygrowth* model can provide a more realistic prior for many infectious disease
374 epidemics where the growth rate of epidemic size is likely to approach stationarity as
375 opposed to the absolute effective population size. Conventional *skyride* and *skygrid* models
376 are prone to erroneously estimating a stable effective population size when genealogical
377 data is uninformative, as for example when estimating epidemic trends in the latter stages
378 of SIR epidemics (Figure 1). The *skygrowth* model will correctly predict epidemic decline
379 in this situation. Moreover, under ideal conditions, the estimated growth rate can be
380 related to the reproduction number of an epidemic, and the *skygrowth* model provides a

381 simple non-parametric estimator of the reproduction number through time given additional
382 information about the natural history of infection (Equation 10). Caution should be
383 exercised when using the effective population size as a proxy for epidemic size, as the
384 relationship between the two is complex (cf. Simulation results). In general, there will be
385 close correspondence between the growth of epidemic size and growth of effective
386 population size during periods where the growth rate is relatively constant.

387 The methods presented here can be applied more generally to evaluate the role of
388 antibiotic stewardship, vaccine campaigns, or other public health interventions on epidemic
389 growth rates. Some environmental covariates, such as independent prevalence estimates,
390 may be more closely related to effective population size rather than growth rates, and
391 future work is indicated on the development of regression models in terms of both
392 statistics. More complex stochastic models can also be considered, such as processes with
393 both autoregressive and moving average components. A variety of mathematical models
394 have been developed to explain de novo evolution of antimicrobial resistance as a function
395 of population-level antimicrobial usage (Bonhoeffer et al. 1997; Austin et al. 1999;
396 Spicknall et al. 2013; Whittles et al. 2017), and an important direction for future work will
397 be the development of parametric and semi-parametric structured coalescent models (Volz
398 2012) that can be applied to bacterial phylogenies featuring a mixture of antibiotic
399 sensitive and resistant lineages. This methodology will allow us to estimate key
400 evolutionary parameters, such as the fitness cost and benefit of resistance, or the rate of
401 mutation from sensitive to resistant status, which are needed to make well informed
402 recommendations on resistance control strategies.

*

403

404 References

- 405 Alam, M. T., T. D. Read, R. A. Petit, S. Boyle-Vavra, L. G. Miller, S. J. Eells, R. S.
406 Daum, and M. Z. David. 2015. Transmission and microevolution of USA300 MRSA in
407 U.S. households: Evidence from whole-genome sequencing. *MBio* 6:1–10.
- 408 Allen, L. 2008. An introduction to stochastic epidemic models. Pages 81–130 *in* *Math.*
409 *Epidemiol.* vol. 1945 of *Lecture Notes in Mathematics*. Springer Berlin Heidelberg.
- 410 Austin, D. J., K. G. Kristinsson, and R. M. Anderson. 1999. The relationship between the
411 volume of antimicrobial consumption in human communities and the frequency of
412 resistance. *PNAS* 96:1152–1156.
- 413 Baele, G., M. A. Suchard, A. Rambaut, and P. Lemey. 2016. Emerging concepts of data
414 integration in pathogen phylodynamics. *Systematic biology* 66:e47–e65.
- 415 Biek, R., J. C. Henderson, L. a. Waller, C. E. Rupprecht, and L. a. Real. 2007. A
416 high-resolution genetic signature of demographic and spatial expansion in epizootic
417 rabies virus. *Proc Natl Acad Sci USA* 104:7993–8.
- 418 Bonhoeffer, S., M. Lipsitch, and B. R. Levin. 1997. Evaluating treatment protocols to
419 prevent antibiotic resistance. *Proc Natl Acad Sci U S A* 94:12106–12111.
- 420 CDDEP. 2017. The Center for Disease Dynamics Economics and Policy. ResistanceMap,
421 available at <http://resistancemap.cddep.org/>, accessed July 2017.
- 422 Chambers, H. F. and F. R. Deleo. 2009. Waves of resistance: *Staphylococcus aureus* in the
423 antibiotic era. *Nat. Rev. Microbiol.* 7:629–41.

- 424 Childs, J. E., A. T. Curns, M. E. Dey, L. A. Real, L. Feinstein, O. N. Bjornstad, and J. W.
425 Krebs. 2000. Predicting the local dynamics of epizootic rabies among raccoons in the
426 United States. *Proc. Natl. Acad. Sci.* 97:13666–13671.
- 427 de Silva, E., N. M. Ferguson, and C. Fraser. 2012. Inferring pandemic growth rates from
428 sequence data. *Journal of The Royal Society Interface* Page rsif20110850.
- 429 Dearlove, B. and D. Wilson. 2013. Coalescent inference for infectious disease: meta-analysis
430 of hepatitis C. *Philos. Trans. R. Soc. B Biol. Sci.* 368:20120314.
- 431 Didelot, X., D. W. Eyre, M. Cule, C. L. C. Ip, M. A. Ansari, D. Griffiths, A. Vaughan,
432 L. O'Connor, T. Golubchik, E. M. Batty, P. Piazza, D. J. Wilson, R. Bowden, P. J.
433 Donnelly, K. E. Dingle, M. Wilcox, A. S. Walker, D. W. Crook, T. E. Peto, and R. M.
434 Harding. 2012. Microevolutionary analysis of *Clostridium difficile* genomes to investigate
435 transmission. *Genome Biol* 13:R118.
- 436 Didelot, X., J. Gardy, and C. Colijn. 2014. Bayesian inference of infectious disease
437 transmission from whole genome sequence data. *Mol. Biol. Evol.* 31:1869–1879.
- 438 Didelot, X., A. S. Walker, T. E. Peto, D. W. Crook, and D. J. Wilson. 2016. Within-host
439 evolution of bacterial pathogens. *Nat. Rev. Microbiol.* 14:150–162.
- 440 Dingle, K. E., X. Didelot, T. P. Quan, D. W. Eyre, N. Stoesser, T. Golubchik, R. M.
441 Harding, D. J. Wilson, D. Griffiths, A. Vaughan, and Others. 2017. Effects of control
442 interventions on *Clostridium difficile* infection in England: an observational study.
443 *Lancet Infect. Dis.* 17:411–421.
- 444 Drummond, A. J., A. Rambaut, B. Shapiro, and O. G. Pybus. 2005. Bayesian coalescent
445 inference of past population dynamics from molecular sequences. *Mol. Biol. Evol.*
446 22:1185–92.

- 447 Drummond, A. J., M. A. Suchard, D. Xie, and A. Rambaut. 2012. Bayesian phylogenetics
448 with BEAUti and the BEAST 1.7. *Mol. Biol. Evol.* 29:1969–1973.
- 449 Fraser, C. 2007. Estimating individual and household reproduction numbers in an emerging
450 epidemic. *PLoS One* 2:e758.
- 451 Frost, S. D. W. and E. M. Volz. 2010. Viral phylodynamics and the search for an 'effective
452 number of infections'. *Phil. Trans. R. Soc. B* 365:1879–1890.
- 453 Gill, M. S., P. Lemey, S. N. Bennett, R. Biek, and M. A. Suchard. 2016. Understanding
454 Past Population Dynamics : Bayesian Coalescent-Based Modeling with Covariates. *Syst.*
455 *Biol.* 65:1041–1056.
- 456 Gill, M. S., P. Lemey, N. R. Faria, A. Rambaut, B. Shapiro, and M. A. Suchard. 2012.
457 Improving bayesian population dynamics inference: a coalescent-based model for
458 multiple loci. *Molecular biology and evolution* 30:713–724.
- 459 Gill, M. S., P. Lemey, N. R. Faria, A. Rambaut, B. Shapiro, and M. A. Suchard. 2013.
460 Improving bayesian population dynamics inference: A coalescent-based model for
461 multiple loci. *Mol. Biol. Evol.* 30:713–724.
- 462 Glaser, P., P. Martins-Simões, A. Villain, M. Barbier, A. Tristan, C. Bouchier, L. Ma,
463 M. Bes, F. Laurent, D. Guillemot, T. Wirth, and F. Vandenesch. 2016. Demography and
464 intercontinental spread of the USA300 community-acquired methicillin-resistant
465 *Staphylococcus aureus* lineage. *MBio* 7:1–11.
- 466 Goldfarb, D. 1970. A family of variable-metric methods derived by variational means.
467 *Mathematics of Computation* 24:23–26.
- 468 Griffiths, R. and S. Tavaré. 1994. Sampling theory for neutral alleles in a varying
469 environment. *Philos. Trans. R. Soc. B Biol. Sci.* 344:403–410.

- 470 Ho, S. Y. and B. Shapiro. 2011. Skyline-plot methods for estimating demographic history
471 from nucleotide sequences. *Molecular ecology resources* 11:423–434.
- 472 Hogeia, C., T. Van Effelterre, and C. J. Acosta. 2014. A basic dynamic transmission model
473 of *Staphylococcus aureus* in the US population. *Epidemiol. Infect.* 142:468–478.
- 474 Karcher, M. D., J. A. Palacios, T. Bedford, M. A. Suchard, and V. N. Minin. 2016.
475 Quantifying and mitigating the effect of preferential sampling on phylodynamic
476 inference. *PLoS computational biology* 12:e1004789.
- 477 Karcher, M. D., J. A. Palacios, S. Lan, and V. N. Minin. 2017. phylodyn: an R package for
478 phylodynamic simulation and inference. *Mol. Ecol. Resour.* 17:96–100.
- 479 Kingman, J. 1982. The coalescent. *Stoch. Process. their Appl.* 13:235–248.
- 480 Koelle, K., O. Ratmann, D. A. Rasmussen, V. Pasour, and J. Mattingly. 2011. A
481 dimensionless number for understanding the evolutionary dynamics of antigenically
482 variable RNA viruses. *Proc. R. Soc. B Biol. Sci.* 278:3723–3730.
- 483 Ledda, A., J. R. Price, K. Cole, M. J. Llewelyn, A. M. Kearns, D. W. Crook, J. Paul, and
484 X. Didelot. 2017. Re-emergence of methicillin susceptibility in a resistant lineage of
485 *Staphylococcus aureus*. *J. Antimicrob. Chemother.* 72:1285–1288.
- 486 McCaig, L. F., R. E. Besser, and J. M. Hughes. 2003. Antimicrobial drug prescription in
487 ambulatory care settings, United States, 1992-2000. *Emerg. Infect. Dis.* 9:432–7.
- 488 McCaig, L. F. and J. M. Hughes. 1995. Trends in antimicrobial drug prescribing among
489 office-based physicians in the United States. *J. Am. Med. Assoc.* 273:214–219.
- 490 Minin, V. N., E. W. Bloomquist, and M. A. Suchard. 2008. Smooth skyride through a
491 rough skyline: Bayesian coalescent-based inference of population dynamics. *Molecular
492 biology and evolution* 25:1459–1471.

- 493 Monroe, B., P. Yager, J. Blanton, M. Birhane, A. Wadhwa, L. Orciari, B. Petersen, and
494 R. Wallace. 2016. Rabies surveillance in the United States during 2014. *J. Am. Vet. Med.*
495 *Assoc.* 248:777–788.
- 496 Palacios, J. A. and V. N. Minin. 2013. Gaussian process-based bayesian nonparametric
497 inference of population size trajectories from gene genealogies. *Biometrics* 69:8–18.
- 498 Planet, P. J. 2017. Life After USA300: The Rise and Fall of a Superbug. *J. Infect. Dis.*
499 215:S71–S77.
- 500 Pybus, O. G. 2001. The Epidemic Behavior of the Hepatitis C Virus. *Science*
501 292:2323–2325.
- 502 Pybus, O. G., A. Rambaut, and P. H. Harvey. 2000. An integrated framework for the
503 inference of viral population history from reconstructed genealogies. *Genetics*
504 155:1429–1437.
- 505 Rosenberg, N. A. and M. Nordborg. 2002. Genealogical trees, coalescent theory and the
506 analysis of genetic polymorphisms. *Nat. Rev. Genet.* 3:380–90.
- 507 Spicknall, I. H., B. Foxman, C. F. Marrs, and J. N. S. Eisenberg. 2013. A modeling
508 framework for the evolution and spread of antibiotic resistance: Literature review and
509 model categorization. *Am. J. Epidemiol.* 178:508–520.
- 510 Strimmer, K. and O. G. Pybus. 2001. Exploring the demographic history of dna sequences
511 using the generalized skyline plot. *Molecular Biology and Evolution* 18:2298–2305.
- 512 Tenover, F. C. and R. V. Goering. 2009. Methicillin-resistant *Staphylococcus aureus* strain
513 USA300: Origin and epidemiology. *J. Antimicrob. Chemother.* 64:441–446.
- 514 Uhlemann, A.-C., J. Dordel, J. R. Knox, K. E. Raven, J. Parkhill, M. T. G. Holden, S. J.
515 Peacock, and F. D. Lowy. 2014. Molecular tracing of the emergence, diversification, and

516 transmission of *S. aureus* sequence type 8 in a New York community. *Proc. Natl. Acad.*
517 *Sci. U. S. A.* 111:6738–43.

518 Vaughan, T. G. and A. J. Drummond. 2013. A stochastic simulator of Birth–Death master
519 equations with application to phylodynamics. *Mol. Biol. Evol.* 30:1480–1493.

520 Volz, E. M. 2012. Complex population dynamics and the coalescent under neutrality.
521 *Genetics* 190:187–201.

522 Volz, E. M. and S. D. W. Frost. 2014. Sampling through time and phylodynamic inference
523 with coalescent and birth – death models. *J. R. Soc. Interface* 11:20140945.

524 Volz, E. M., K. Koelle, and T. Bedford. 2013. Viral Phylodynamics. *PLoS Comput. Biol.*
525 9:e1002947.

526 Volz, E. M., S. L. Kosakovsky Pond, M. J. Ward, A. J. Leigh Brown, and S. D. W. Frost.
527 2009. Phylodynamics of infectious disease epidemics. *Genetics* 183:1421–30.

528 Volz, E. M., E. Romero-Severson, and T. Leitner. 2017. Phylodynamic Inference across
529 Epidemic Scales. *Mol. Biol. Evol.* 34:1276–1288.

530 Whittles, L., P. White, and X. Didelot. 2017. Estimating the fitness cost and benefit of
531 cefixime resistance in *neisseria gonorrhoeae* to inform prescription policy: a modelling
532 study. *PLoS Medicine* .